

Voyager color photometry of Saturn's main rings: a correction [☆]

Paul R. Estrada,^a Jeffrey N. Cuzzi,^{a,*} and Mark R. Showalter^b

^a *Space Science Division, Ames Research Center, NASA, MS 245-3, Moffett Field, CA 94035-1000, USA*

^b *Stanford University, Stanford, CA 94305, USA*

Received 16 August 2002; accepted 20 June 2003

Abstract

We correct a calibration error in our earlier analysis of Voyager color observations of Saturn's main rings at 14° phase angle (Estrada and Cuzzi, 1996, *Icarus* 122, 251) and present thoroughly revised and reanalyzed radial profiles of the brightness of the main rings in the Voyager green, violet, and ultraviolet filters and the ratios of these brightnesses. These results are consistent with more recent HST results at 6° phase angle, once allowance is made for plausible phase reddening of the rings (Cuzzi et al., 2002, *Icarus* 158, 199). Unfortunately, the Voyager camera calibration factors are simply not sufficiently well known for a combination of the Voyager and HST data to be used to *constrain* the phase reddening quantitatively. However, some interesting radial variations in reddening between 6 and 14° phase angles are hinted at. We update a ring-and-satellite color vs albedo plot from Cuzzi and Estrada (1998, *Icarus* 132, 1) in several ways. The A and B rings are still found to be in a significantly redder part of color-albedo space than Saturn's icy satellites.

© 2003 Elsevier Inc. All rights reserved.

1. Motivation

As part of our recent analysis of the phase and opening angle dependence of ring brightness using Hubble Space Telescope (HST) data between 0 and 6° phase angle, we realized that the redness of the rings increases with phase angle but is independent of ring opening angle (Cuzzi et al., 2002, henceforth CFD02). However, we found that our earlier Voyager measurements at the higher phase angle of 14° (Estrada and Cuzzi, 1996, henceforth EC96) fell well off the HST trend and appeared anomalously red. Poulet et al. (1999), unaware at the time of the phase reddening effect, had independently noted a quantitative discrepancy between the EC96 data and their earlier, lower resolution and lower phase angle WF/PC data. Because the HST data show extremely interesting and puzzling spatial color variations (Cuzzi et al., 2000) that can be studied in the Voyager data at much higher spatial resolution, we felt it necessary to revisit the earlier EC96 analysis to resolve these discrepancies. Indeed, we found a calibration error and one other inappropriate correction technique. Below, we describe the completely new reanalysis of these data, which replaces that

in EC96; however, we refer the reader to the calibration discussion in EC96 and will not repeat most of it here.

2. Description of new procedure

2.1. Voyager calibration

We will discuss the Voyager green (G), violet (V), and ultraviolet (UV) filters. The sensitivity of the Voyager cameras is described by the camera calibration factors w_0 , which relate the ring brightness I/F to the data number ΔDN resulting after integration time t seconds, as $I/F = \Delta DN / (w_0 t)$. As discussed in EC96, there are uncertainties in the calibration of the Voyager filters that remain even today. The original calibration factors $w_0(\lambda)$ (and the only officially published ones) are the “Danielson” calibration factors (Danielson et al., 1981). Recalibration of the cameras in flight using two different data sets led to “atmospheric” and “satellite” calibration factors (described in EC96). These latter two differ only for the UV filter, for which the Voyager Imaging Team merely averaged the two values to obtain the so-called “Johnson–Buratti” or JB calibration. These factors are not officially published by their creators anywhere; however, all the relevant calibration factors are given for the Voyager 2 Narrow Angle Camera in EC96, and a more complete set is available from the PDS Rings Node (Showalter et al., 1996).

[☆] PII of original article: S0019-1035(96)90124-4.

* Corresponding author.

E-mail address: jcuzzi@mail.arc.nasa.gov (J.N. Cuzzi).

All these more recent calibrations show the cameras to be about 8% more sensitive in G and about 12% less sensitive in UV than under the Danielson calibration, reducing the I/F inferred from G filter data and increasing that inferred from UV filter data. Note that the calibration used by Buratti (1984) to obtain the colors we adopted for Mimas and Enceladus is actually different from, and superceded by, the JB calibration, and we correct for that here.

Our primary reduction averages pixel brightnesses along ring contours to create profiles, or “scans,” of ring brightness or I/F . In our prior analysis of the Voyager color images, we unwittingly applied the Danielson calibration to our primary reduction in spite of our stated intent to apply the JB calibration. We then corrected the UV scans to the atmospheric calibration, for reasons discussed in EC96. However, because we believed the scans to incorporate the JB calibration, we corrected them by a factor of $(w_{0,\text{JB}})/(w_{0,\text{atm}})$ instead of the more appropriate correction factor $(w_{0,\text{Dan}})/(w_{0,\text{atm}})$. Thus, for instance, the published ratios of G/UV brightness ratio were high by factors of

$$\begin{aligned} & \left(\frac{(w_{0,\text{JB}})/(w_{0,\text{atm}})}{(w_{0,\text{Dan}})/(w_{0,\text{atm}})} \right)_{\text{G}} \bigg/ \left(\frac{(w_{0,\text{JB}})/(w_{0,\text{atm}})}{(w_{0,\text{Dan}})/(w_{0,\text{atm}})} \right)_{\text{UV}} \\ &= \frac{(w_{0,\text{JB}})/(w_{0,\text{Dan}})_{\text{G}}}{(w_{0,\text{JB}})/(w_{0,\text{Dan}})_{\text{UV}}} = 1.28. \end{aligned}$$

2.2. Background subtraction

As part of the reanalysis reported here, we made use of comparisons with the newer HST data and found differences that indicated some of our background subtraction had also been inappropriate. The images we analyzed were all Voyager Narrow Angle (NAC) frames, and three image pointings were required to cover one ansa of the main rings. The actual “dark sky background” was really only seen outside the A ring and inside the C ring. From inspection and known resolution, we believed that there were several narrow gaps in the Cassini Division and C ring which were adequately resolved to be good measures of true “dark sky.” In retrospect, this seems not to have been the case, because the radially variable background correction led to inconsistency with the HST color results. The simplest thing to do is simply subtract a constant background for each frame, and this is what we have done here. The B ring scan has no usable dark sky for determination of its own background, but using a constant background value aligns the B ring radial I/F scan at both ends with the adjacent A and C ring scans. I/F scans presented here have had only a constant background I/F subtracted, as follows: A ring: 0.0025 in G, 0.0045 in V, and 0.0075 in UV; B ring: -0.0015 in G, and 0.002 in V; C ring: -0.005 in G, -0.0023 in V, and -0.0024 in UV. The B ring UV scan lined up well with both the A and C rings and required no registration correction.

2.3. Use of Voyager Wide Angle frames as check

One additional check we implemented here that was not done in EC96 was to make use of several nearly simultaneous Voyager Wide Angle Camera (WAC) images to check the overall alignments and background subtractions. The WAC resolution (10 times worse than the NAC) is better than our recent HST image data, and quite capable of establishing the overall I/F profiles. The WAC ring images were completely surrounded by dark sky so background determination is simple, and of course registering scans taken in different parts of the rings is not an issue. Unfortunately, there is no UV filter on the WAC. It is of interest that the WAC G filter is very similar to the NAC G filter, but the WAC V filter has a distinctly longer effective wavelength (approximately 430 nm) than the NAC V filter (approximately 415 nm) (see Fig. 1; data available on PDS Rings Node). This allows ring color effects, and their variation with radius, to appear between the WAC and NAC V filter profiles. After taking the WAC scans in G and V filters and correcting them from the Danielson calibration to the JB calibration,¹ we smoothed our NAC scans to similar resolution, radially shifted the WAC scan to fit, and ratioed the scans (see Fig. 2).

In Fig. 2, the large noiselike fluctuations in the inner and outer C ring (near 80,000 and 90,000 km) and in the Cassini Division and Encke gap regions (120,000 and 133,000 km) are associated with narrow ring features which suffer from residual misregistrations and the poorly known WAC point spread function. Aside from these known discrepancies, the

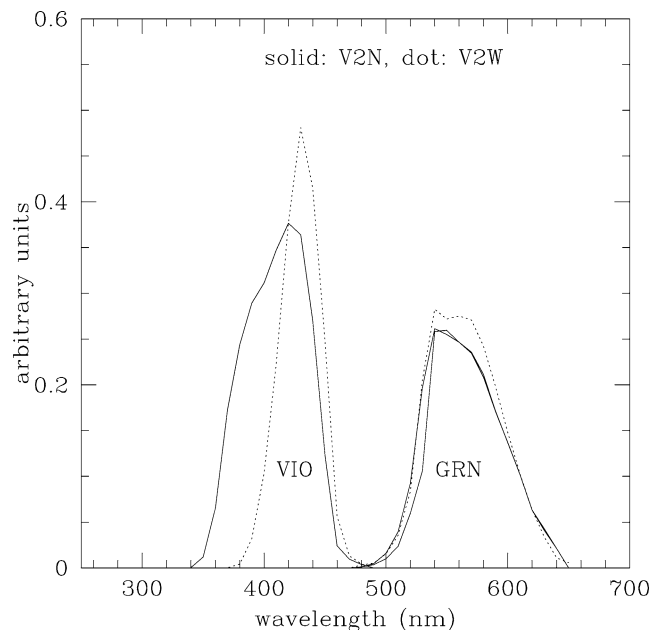


Fig. 1. Comparison of green and violet filter responses for the Voyager 2 WAC (dotted curves) and NAC (solid curves). The VIO filters are significantly different over a spectral range where the rings are quite red.

¹ The JB calibration factors for the Voyager 2 WAC are $w_0(\text{V}) = 729.270$; $w_0(\text{G}) = 1112.14$.

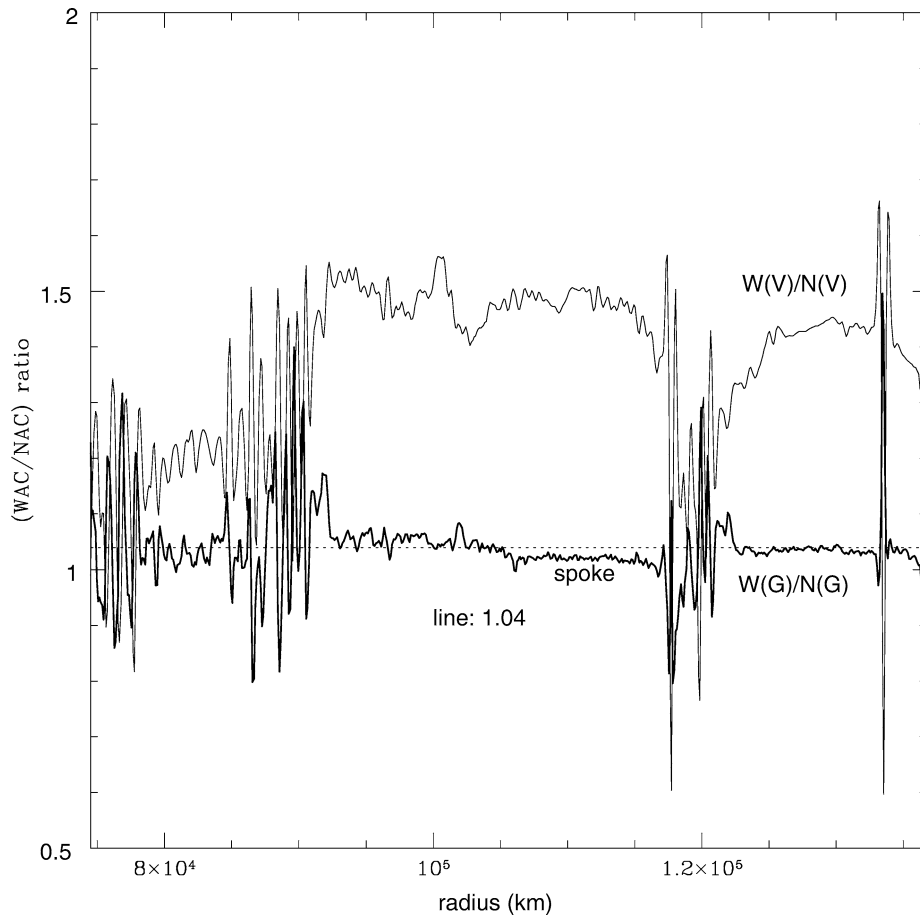


Fig. 2. Radial ratio profiles of brightness scans taken from Voyager 2 WAC and NAC images in green and violet filters. Large noiselike fluctuations in the inner and outer C ring (near 80,000 and 90,000 km) and in the Cassini and Encke gap regions (120,000 and 133,000 km) are associated with narrow features which suffer from residual misregistrations and the poorly known WAC PSF. Aside from these known discrepancies, the WAC/NAC profile in the green filter is quite flat (except for one identified region in which the WAC contained a spoke). On the other hand, the WAC/NAC profile in the respective violet filters shows the same sort of radial structure as seen globally between different filters (EC96). This is readily ascribed to the different wavelength coverage of the WAC and NAC violet filters.

WAC/NAC profile in the green filter is quite flat (except for one identified region in which the WAC contained a spoke). This test provided a guarantee that no serious intensity mismatch occurred where our three different NAC image scans (of the A, B, and C rings) were pieced together to create full radial profiles. Quantitatively, there is a radially independent 4% discrepancy between the WAC and NAC G filter scans. This is probably at the ultimate limit of Voyager filter calibration.

In contrast, the V filter ratios have an appearance similar to that of our other color ratios—differing noticeably between the C ring, Cassini Division regions, and the A, B ring regions—and even within the A and B rings themselves in a fashion completely consistent with actual spectral variations. This is readily ascribed to the different wavelength coverage of the WAC and NAC violet filters. This difference between the Voyager WAC and NAC V filters provides another spectral window into the rings, which might be worth pursuing in future work; herein, we remain focused on the highest spatial resolution (NAC) data.

2.4. All smear and radial shift adjustments redone for good measure

While doing this reanalysis, we decided to redo all the fine adjustments from scratch. Fine adjustment of scans was needed for two reasons. First, none of the UV images of the C ring were unsmear. We selected the best one, but in order to take color ratios, we needed to smear the G and V scans of the C ring commensurably. This trial-and-error process was refined to allow for an effective smear in the inner B ring slightly different from that in the C ring (due to variation of ring curvature across the field of view). Smear was by a boxcar filter with a half width of 3.5 pixels for the C ring and 2.5 pixels for the inner B ring. The pixel width was 12.5 km at this time. Second, artifacts in the ratio profiles, caused by incorrect radial shifts, are easily recognized as asymmetrical peak-and-valley features near sharp edges in the I/F profiles and can be easily removed by small radial shifts. To avoid introducing too many free parameters, we used a single radial shift for each ring and a separate shift for two specific regions where we have reason

to believe that the routine camera geometric correction might have been inadequate. Although the standard Voyager geometric correction is supposed to remove camera distortions, it is often imperfect in the periphery of images. The outer A ring (outside the Encke gap) and the Cassini Division both fell near the periphery of the A and B ring images, and both regions required separate (but constant) radial shifts to align them best between different images. The separately shifted regions were rejoined to the rest of the scan in empty gaps that separate them.

3. Results

The final result is a set of three entirely new, fully self consistent merged radial profiles of ring I/F in Voyager G, V, and UV filters, calibrated following the Voyager atmospheric standard. Associated with this is a set of three profiles obtained by taking ratios of the I/F profiles, cleaned up only by removing the one or two residual edge-

mismatch artifacts at the Maxwell gap/ringlet and Huygens gap/ringlet, as well as the inner and outer ring edge regions, and the C ring gaps.

3.1. Selected color differences on small scales

The data for the A, B, and C rings are shown in Figs. 3–5. Details of the Cassini Division and outer C ring are shown in Figs. 6 and 7. One new result emerged from this reanalysis. It appears that there is a real color difference between the outer C ring “plateau” features and their surroundings and that the cause of this is some additional UV absorber in the plateau material. There is little or no evidence for any spectral changes between G and V, but there are clear differences in both G/UV and V/UV across these features (Figs. 3 and 7). Some small edge effects remain, but the plateau color differences are not due to edge effects; the plateaus are more absorbing in the UV than their surroundings, in a relative sense. Similar effects in other rings are under study.

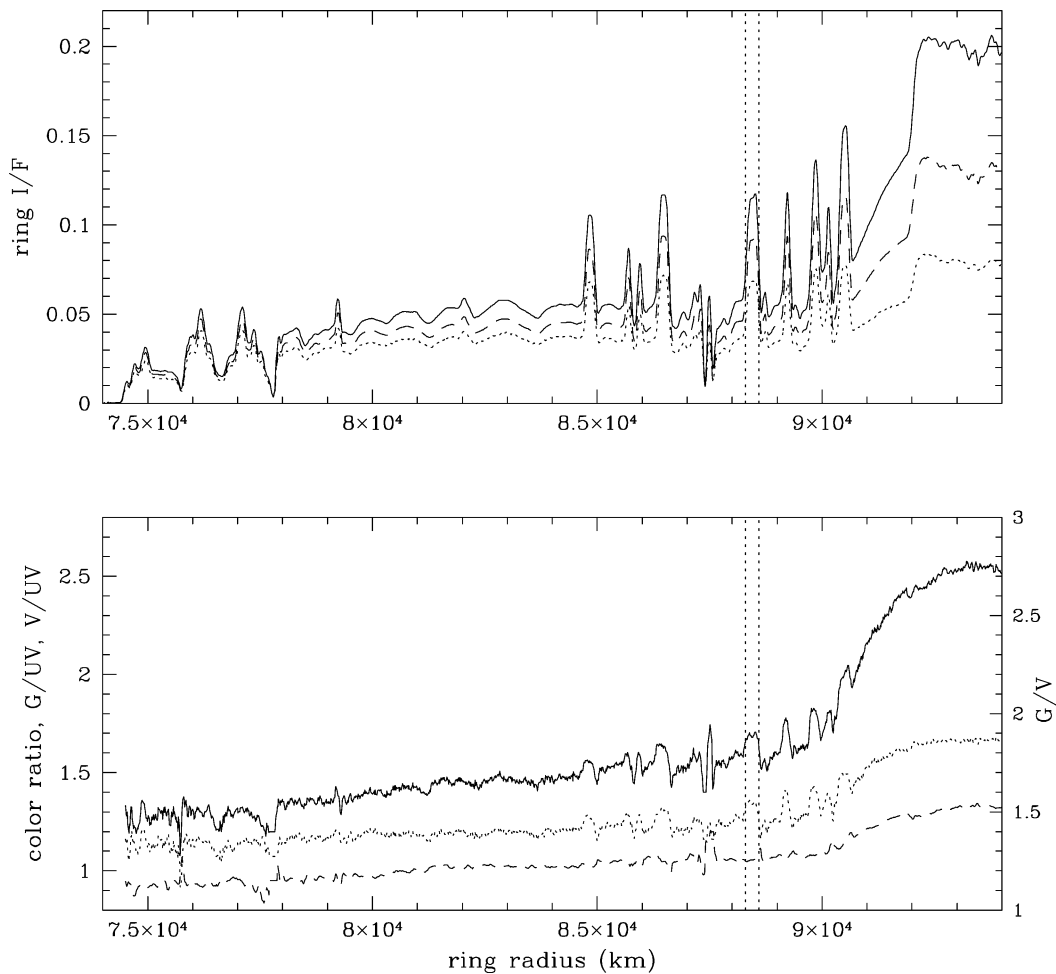


Fig. 3. C ring brightnesses (I/F , top) and their ratios (bottom). In the upper panel, solid line = G filter, dashed line = V filter, and dotted line = UV filter. In the lower panel, solid line = G/UV, dashed line = G/V, and dotted line = V/UV.

Note. The right vertical axis scale corresponds to the G/V ratio. This has been offset by 0.2 vertically relative to the left axis for clarity. Vertical dotted lines identify color differences associated with optically thicker “plateau” features; see also Fig. 5.

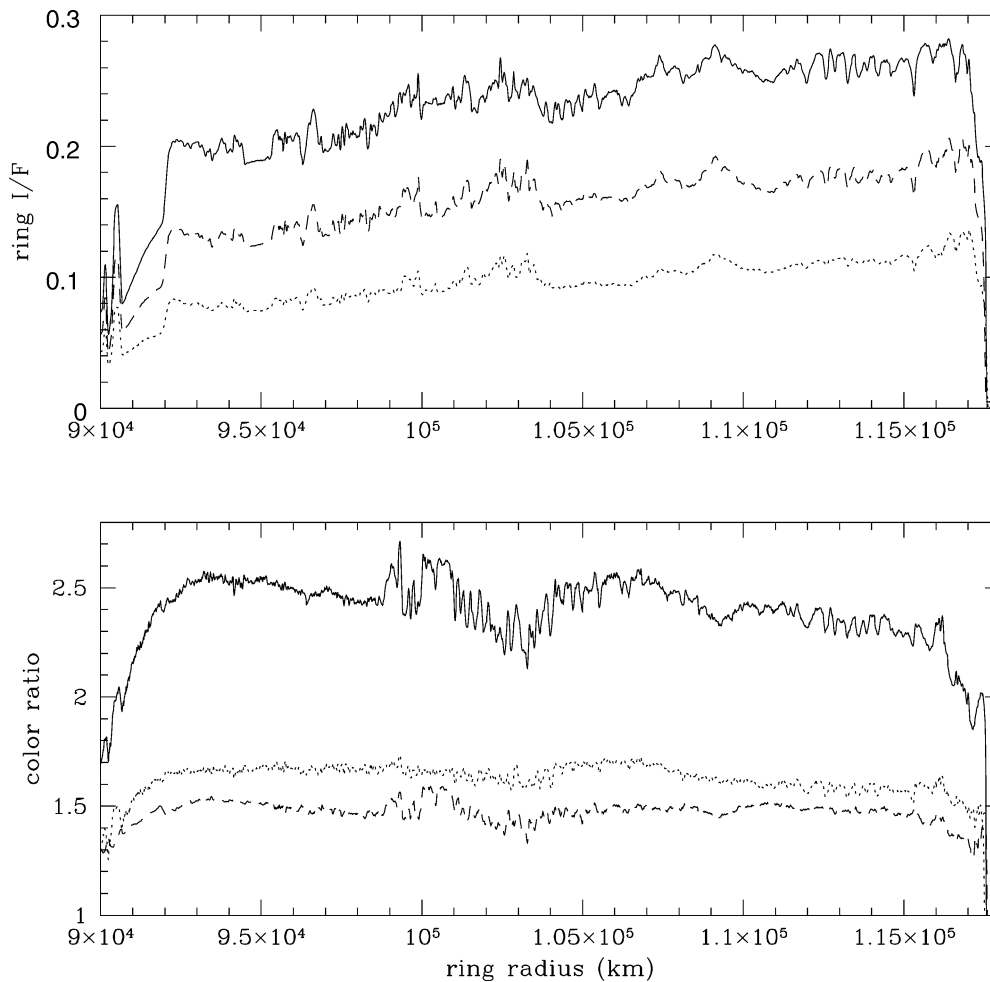


Fig. 4. B ring brightnesses (I/F , top) and their ratios (bottom). In the upper panel, solid line = G filter, dashed line = V filter, and dotted line = UV filter. In the lower panel, solid line = G/UV, and dashed line = G/V, and dotted line = V/UV.

3.2. Caveats

Some narrow features appear to have unusual color ratios: the Maxwell ringlet at 87,500 km and the Huygens ringlet at 117,850 km. While we have taken pains to best allow for smearing and registration, and believe that all features with width greater than 100 km are well represented by these ratios, we remain skeptical that the color ratios seen for these two narrow features are real. A more careful treatment of these features, separately, might be needed in the future.

3.3. Calibration issues

The Voyager calibration remains uncertain overall. The very fact that the atmospheric and satellite calibrations, done carefully by their different advocates, differ by 14% in the UV filter indicates an uncertainty for that filter that may be as large as their difference. For the other filters, the 4% agreement between the WAC and NAC green filter scans may be taken as an estimate of calibration accuracy. As before, we feel that the atmospheric calibration is preferable—at least

for extended objects—because under the satellite calibration, the reddening trend seen in HST data between 0.3° and 6.0° actually reverses by the Voyager 14° phase angle—implying that the C ring is *less red* than at smaller phase angles. We believe this is inconsistent with plausible behavior, in which simple models predict the rings will continue to redden (Poulet et al., 2002a), and we prefer the atmospheric (redder) calibration for this reason. However, due to the UV filter calibration uncertainty, it is impossible to utilize the Voyager color ratios to constrain the phase behavior of ring color (see, e.g., Poulet et al., 2000, 2002a). Several options exist: One might base reddening models on the better calibrated violet/green pair, and drop the less-well-calibrated UV data for this purpose. Or, it might be possible to tie together the lowest phase angle Voyager 2 images, taken at less than 7° phase several months before encounter and never analyzed, with the highest phase angle HST images (6° phase), to better constrain the Voyager calibration scale at the UV wavelengths where considerable uncertainty remains.

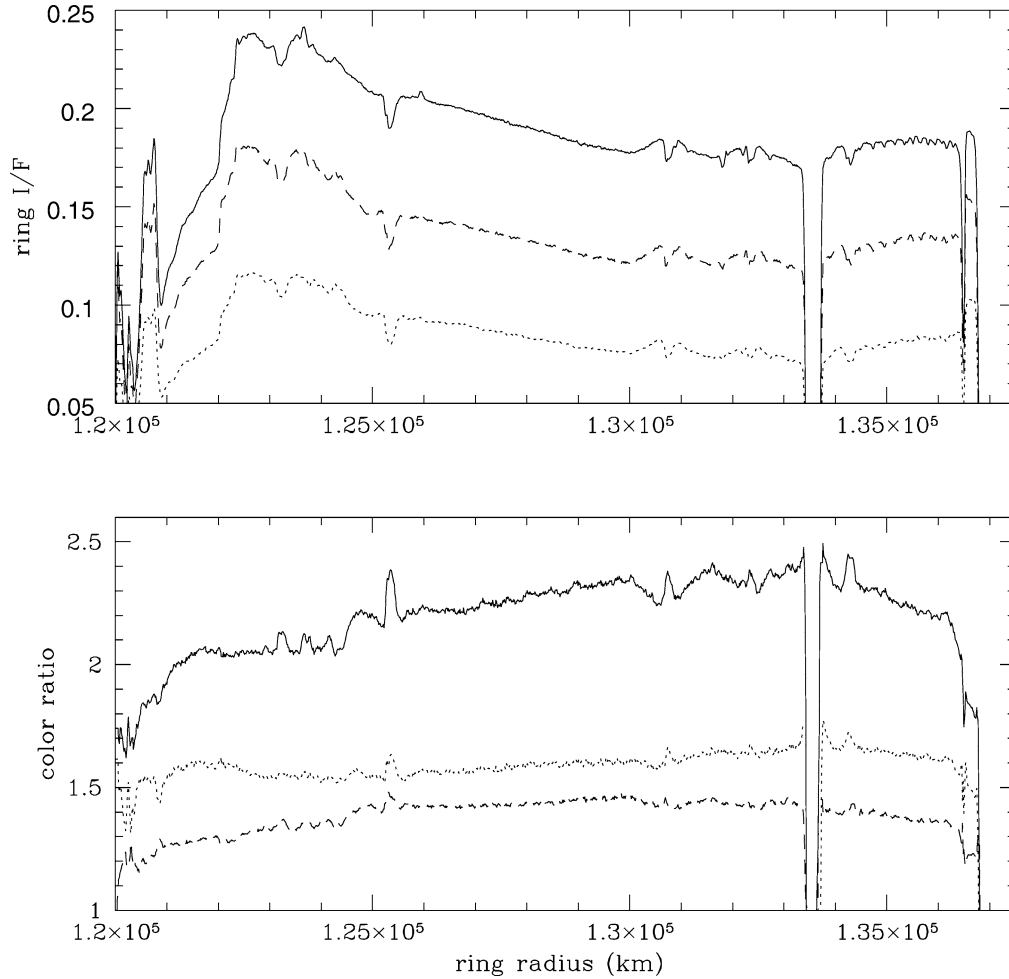


Fig. 5. A ring brightnesses (I/F , top) and their ratios (bottom). In the upper panel, solid line = G filter, dashed line = V filter, and dotted line = UV filter. In the lower panel, solid line = G/UV , dashed line = G/V , and dotted line = V/UV .

3.4. Possible radial variation in phase reddening

In spite of the calibration uncertainties, the data are probably good enough to reveal *radial variations in phase reddening*, simply by taking ratios of HST and/or Voyager radial profiles at different phase angles. CFD02 have noted that Sun and Earth elevation angles seem to have negligible effects on color ratios in this (generally backscattering) geometry. Figure 8 shows in the bottom panel the radial profiles of HST F555W/F336W brightness at three phase angles (0.5° , 2.0° , and 6.0°), each set containing curves from several different ring opening angles from 4° to 20° (discussed in detail by CFD02). Also in the bottom panel is the Voyager G/UV profile, formed from individual Voyager G and UV profiles smoothed by the HST PSFs (CFD02). The upper panel shows ratios of these curves to each other, representing relative changes in redness between 0.5° and 2.0° , 2.0° and 6.0° (both dotted, from HST data), and 6.0° and 14° (solid, from the Voyager/HST(6°) ratio). The dotted curves are consistent with each other and show the C ring to have a slightly smaller phase reddening than the B and A

rings. CFD02 interpreted this as a particle surface effect, and Poulet et al. (2000, 2002a) have shown that surface effect to be a combination of intrinsic redness and macroscopic facet roughness. Considering the Voyager/HST profile, the large dip near 90,000 km is attributable to residual HST scattered light issues, and the smaller dip near 105,000 km is known spoke contamination. Other than that, the profile shows a noticeable upward radial trend, with the A ring appearing to become redder between 6° and 14° phase than the B ring. Poulet et al. (2002a) have shown that the phase reddening of the rings overall can be ascribed to multiple *intraparticle* scattering, or illumination of shadowed facets by illuminated ones. The degree of surface roughness required to fit the magnitude of the effect is significantly larger than that for a scaled-down satellite-type object, consistent with the expectation that the ring “particles” are clumpy aggregates of smaller particles. In the context of Poulet et al. (2002a), the continually increasing redness of the A ring would be consistent with the A ring particles being “lumpier” than the B ring particles.

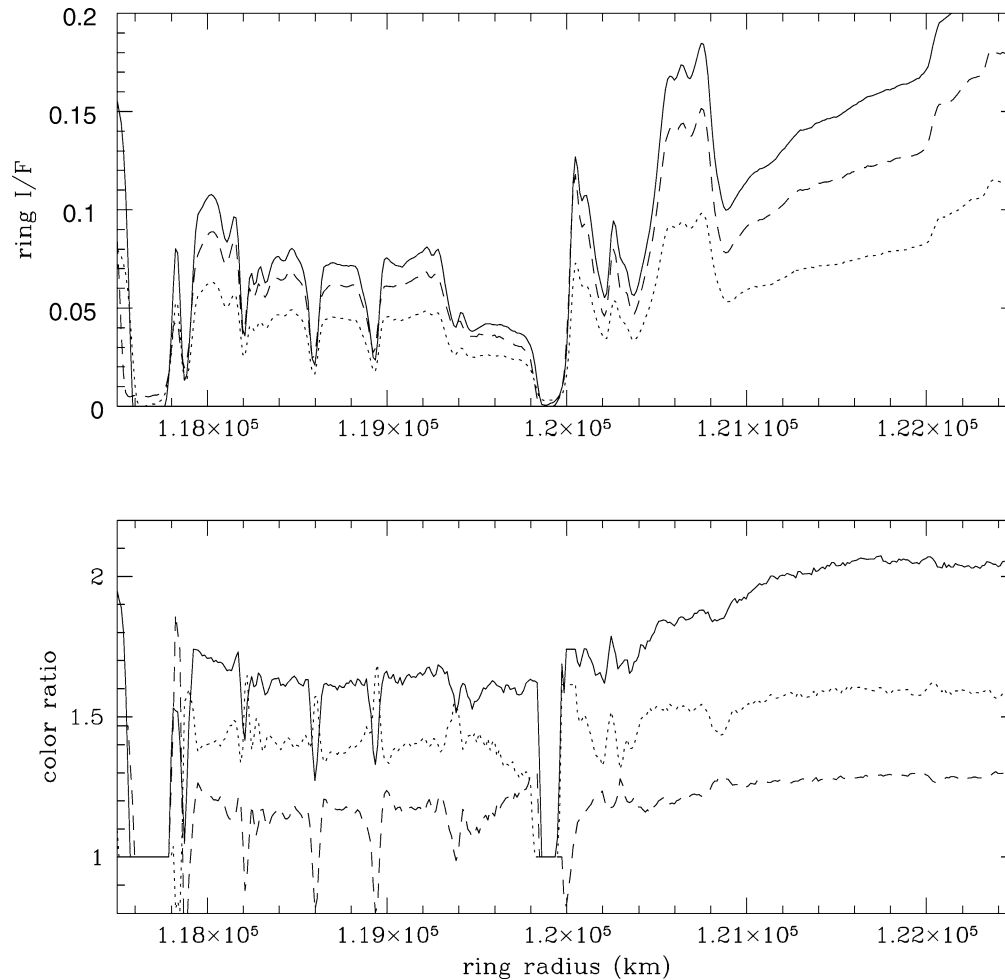


Fig. 6. Cassini Division brightnesses (I/F , top) and their ratios (bottom). In the upper panel, solid line = G filter, dashed line = V filter, and dotted line = UV filter. In the lower panel (color ratios) solid line = G/UV, dashed line = G/V, and dotted line = V/UV. Note that, in contrast to the outer C ring region, “plateau” features here seem to show no color differences from their surroundings. Apparent color differences associated with the Huygens ringlet at 117,850 km are questionable.

3.5. Implications

A comparison of the color-albedo properties of the nominal ring regions of Cuzzi and Estrada (1998, hereafter CE98) ($1.4R_s$ and $1.6R_s$) and the newly added A ($2.15R_s$) and outer B ($1.85R_s$) rings with comparable properties of various icy satellites is shown in Fig. 9 (a revision of CE98 Fig. 3). The clear filter albedos A_c for the C and inner B rings were obtained as described by CE98. The value of A_c for the outer B ring was taken from Doyle et al. (1989), and that for the A ring from Dones et al. (1993). The satellites of Saturn are shown as circles; newer values from Noll et al. (1997) have replaced some older values (dotted circles); the differences are only very slight. Furthermore, a check of Buratti (1984) revealed that the color calibration factors used there actually differed from the Johnson–Buratti set, requiring an adjustment of the G/UV ratio for the Mimas and Enceladus G/UV ratios from CE98 (dotted circles) by a factor of 1.16 (solid circles for M, E). Adopting our preferred “atmospheric” calibration for the Buratti (1984) Mimas and Enceladus

data moves those points to the dashed circles in Fig. 9. None of these updates changes the basic story of the color-albedo ranges of the icy satellites relative to that for the rings. The jovian satellites are redder than Saturn’s icy satellites, but less red than the rings. The most recent groundbased (spectroscopic) colors of the galilean satellites (Spencer et al., 1995) are quite a bit redder than those in the filterband photometry by McFadden et al. (1980). However, J. Spencer (personal communication, 2002) feels that the uncertainties in their spectroscopic technique at short wavelengths leave the older data as more reliable.

The redness of the rings has been reduced relative to that presented by CE98 by two effects. First, the calibration error discussed here reduced the G/UV ratios by 28% (to values shown by the dotted squares). Second, the phase reddening effect discovered by CFD02 and analyzed by Poulet et al. (2002a) implies that the Voyager results (at 14° phase) should not be compared with the satellite geometric albedo data; rather, we use the HST results at 0.3° phase (solid squares) as a conservative lower limit on the redness. Both

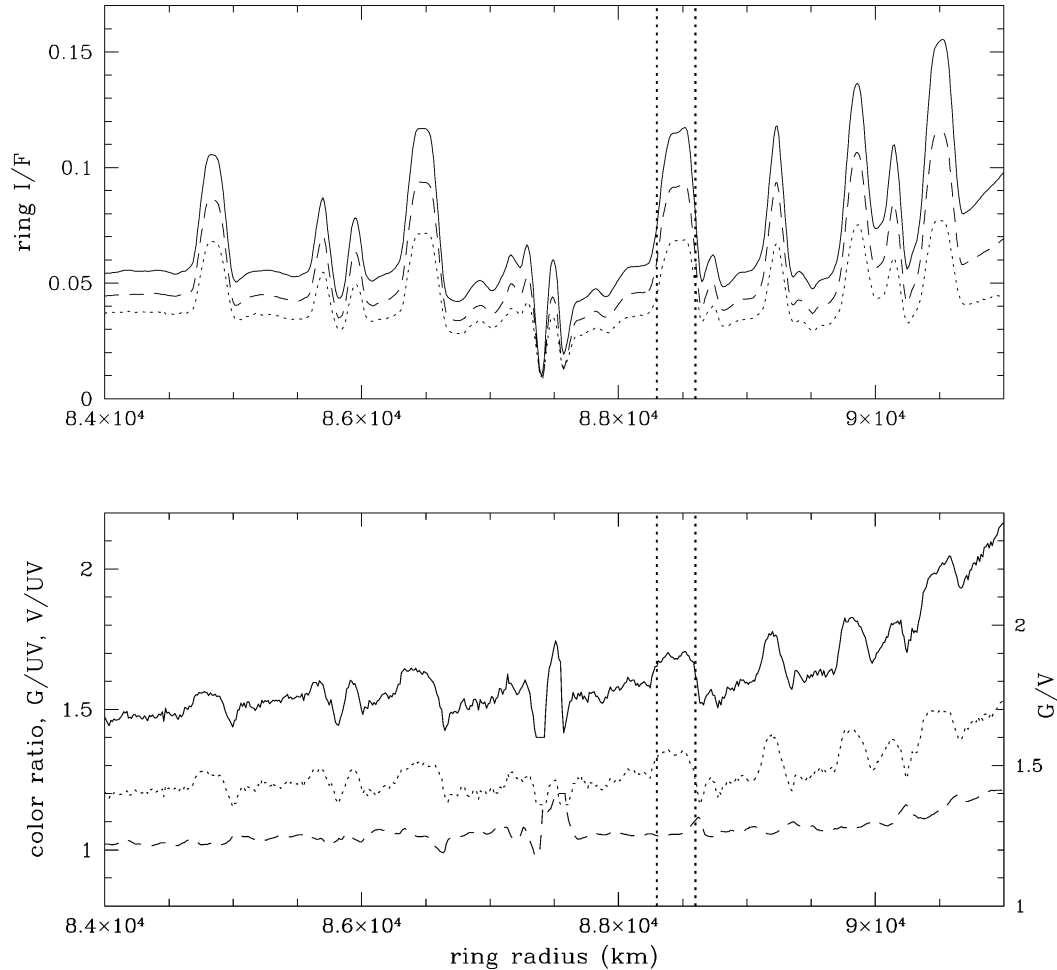


Fig. 7. C ring detail (I/F , top), showing how the outer C ring plateau features are associated with relatively large G/UV and V/UV ratios, but show no spectral difference in their G/V ratios. In the upper panel, solid line = G filter, dashed line = V filter, and dotted line = UV filter. In the lower panel (color ratios), solid line = G/UV , dashed line = G/V , and dotted line = V/UV .

Note. The right vertical axis scale corresponds to the G/V ratio. This has been offset by 0.2 vertically relative to the left axis for clarity. Apparent color differences associated with the Maxwell ringlet at 87,500 km are questionable.

the A and B rings remain distinctly redder than the ensemble of Saturn's icy moons, which CE98 interpreted as evidence for origin of the B ring from tidal disruption of an extrinsic heliocentric interloper containing organic material in its icy mantle rather than from impact disruption of a locally formed object with the more neutral colors of the icy satellites. In fact, the A and B rings still seem unusually red even compared to the satellites of Jupiter (except for Io, of course). Poulet and Cuzzi (2002) produced a new radiative transfer analysis of the main rings, using the average ring spectrum of Karkoschka (1994) and exploring a wide range of compositional phase space. They found that Tholin-like organics could represent between 0.02 and 3.5% of the rings, depending on how it was distributed. This is consistent with the original findings of CE98 (0.4% of organics) showing that model uncertainties dominate calibration uncertainties.

The dotted grid in Fig. 9 represents lines of constant *imaginary index of refraction* (the straight lines, with absorption increasing downward) and *redness slope* of the imag-

inary index (curved lines, with redness increasing to the right). Each curved line is a “trendline” in (A_c, \mathcal{R}) space traversed by a particle of some intrinsic redness to which spectrally neutral material is added (moving the (A_c, \mathcal{R}) point downward along a curved line). The specific *values* of these parameters depend on the regolith grain model (see CE98 for further discussion), but the qualitative behavior is insensitive to the model. Note how the icy satellites of Saturn are scattered along a trendline at the left of the diagram, which is in fact a trendline having little or no intrinsic reddening agent present.

CE98 had suggested that since the C ring color was redder than the icy satellite colors, it could be best explained by adding neutral, or slightly bluish, material to the unusually red B ring material (trendline moving slightly to the left from a neutral trendline). This remains an option, but now the C ring material cannot be so easily distinguished from material present on the surfaces of the icy moons and might even share *their* evolutionary trendline rather than deriving from the B ring material. It seems as if the A ring point can

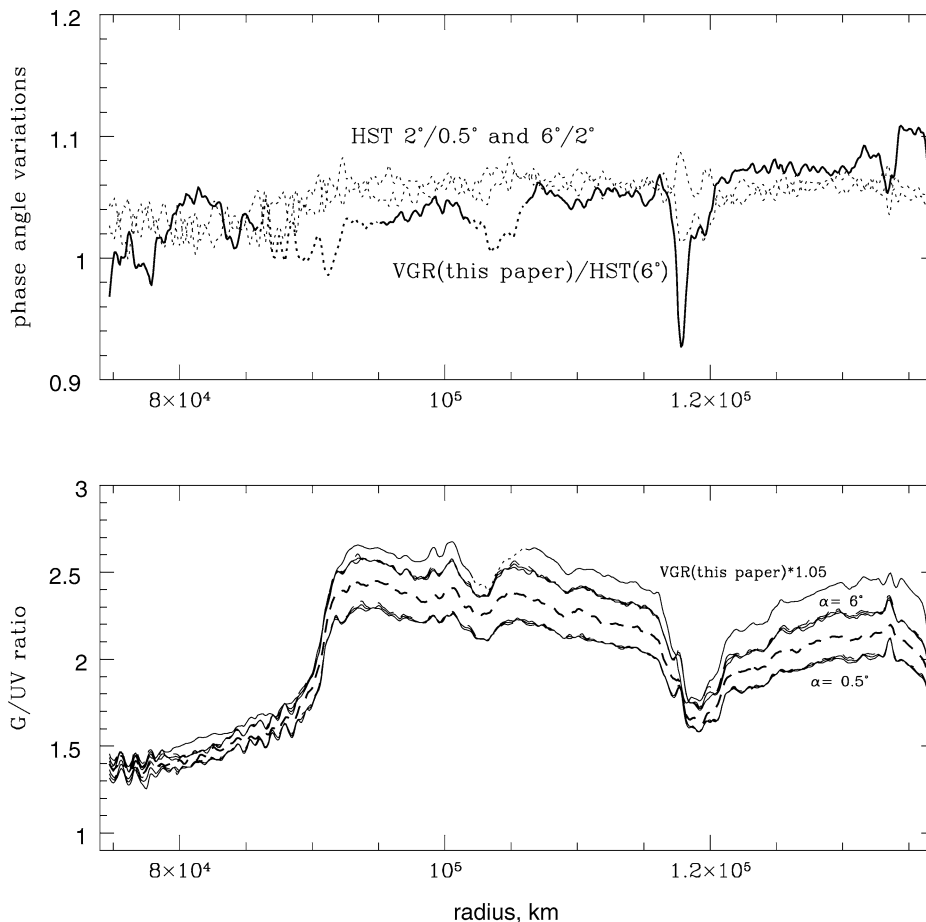


Fig. 8. Comparison of two kinds of ratios involving HST and VGR data at phase angles of 0.5° , 2° , 6° (HST), and 14° (VGR). In the upper panel, the ratio of the HST(2°)/HST(0.5°) and the HST(6°)/HST(2°) (both dotted) show a slightly larger reddening for the A and B rings than for the C ring. The phase reddening between HST (6°) and Voyager (14°) (heavy solid curve) is unknown to a constant of order unity, but there does seem to be a significant radially outward increase in phase reddening across the B and A rings, in addition to the C ring difference. In the VGR/HST(6°) curve, both the spoke-contaminated region and a possible artifact due to inadequate scattered light correction (Cuzzi et al., 2002) are shown dotted. In the lower panel, the color ratios are shown for HST and VGR data. The HST set contains several different ring opening angles at each phase angle (overlapping curves). In the VGR (14°) curve (top profile) the dotted segment represents spoke contamination in one but not both images. The VGR data set is multiplied by 1.05 for visibility. There may still be truth in this factor, if the rings continue to redden to larger phase angles as expected (see text; Results).

be understood as moving down a trendline from the outer B ring material as a result of adding neutral material. It seems reasonable that the more opaque regions of the ring (generally represented by the outer B ring point) are more resistant to evolutionary modification and represent the initial composition better than the optically thinner A or inner B ring material.

However, the C, A, inner B, and outer B ring regions do not share a common trendline. Thus an evolutionary approach to understanding the differences between the inner and outer B ring material, the A ring material, and the C ring material will apparently need to rely on more than one added constituent or evolutionary process. If one postulates an evolutionary process by which rings become redder, then one must leave open the possibility that the redness of the rings relative to that of the icy satellites might itself be an evolutionary effect. In principle, this might allow the rings to have started out with the same composition as the moons. However, if this was the case, one must wonder why the

C ring remains essentially unreddened. Overall, the significant distinction between color of the A and B rings and Saturn's icy satellites of the same albedo is a fact that must be dealt with in understanding the origin and evolution of the rings.

The HST data will remain a critical tiepoint to low-phase-angle “true” colors, and already manifest a very surprising and complex variation of color with location and ring optical depth (Cuzzi et al., 2000). As a next step, we hope to take a much closer look at the Voyager data for trendline-type evolutionary connections. The Voyager data have 10 times higher spatial resolution than the HST data, and we now have it in three well-calibrated filters.

Acknowledgments

This work was supported in part by NASA Planetary Geology and Geophysics Program grants to J. Cuzzi,

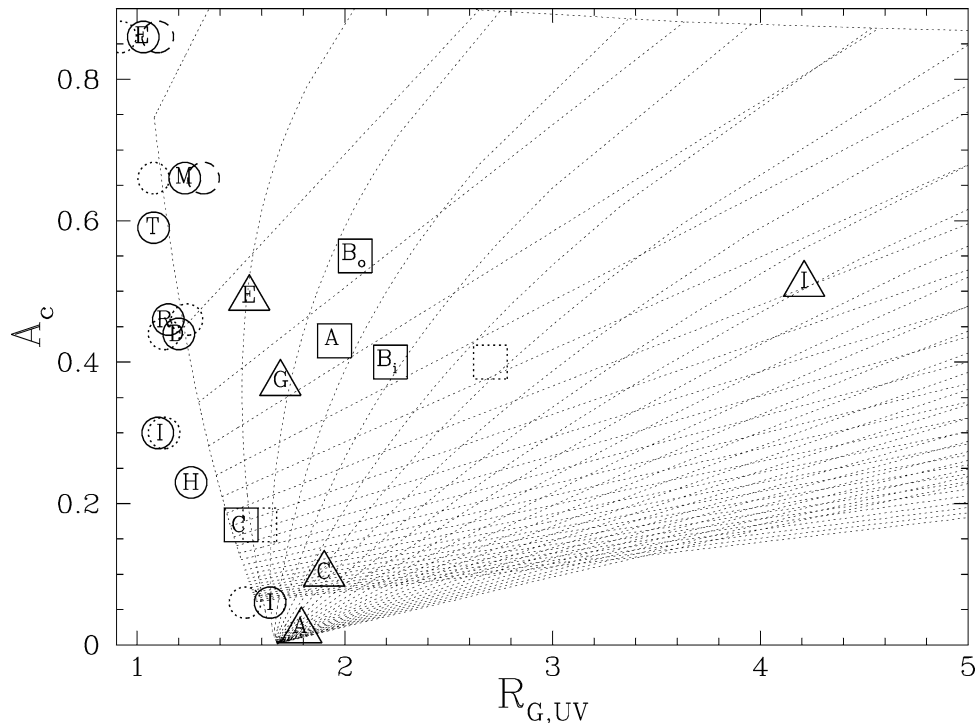


Fig. 9. Revised version of the albedo-color space presented by CE98 (their Fig. 3). Typical mid-A, inner and outer B, and mid-C ring regions are denoted by squares. Dotted squares reflect the Voyager values corrected for the EC96 calibration error, but at 14° phase angle; solid symbols are from the HST data at 0.3° phase angle, which are more appropriate for comparison with low-phase-angle measurements of satellites. The two squares for the B ring represent the colors near the inner and outer edges, at 1.60 (B_i) and $1.85 R_s$ (B_o). The A ring square is near $2.15 R_s$, with A_c from Dones et al. (1993). Saturn's icy satellites are shown by circles. Recent observations of Rhea, Dione, and Iapetus (Noll et al., 1997), shown as solid circles, change the values from those adopted by CE98 (dotted circles) only slightly. No new observations of Mimas, Enceladus, Hyperion, or Tethys are available, but the Mimas and Enceladus values have been corrected here to make their calibration consistent with the Voyager JB calibration system (see text). The jovian satellites are shown by triangles (McFadden et al., 1980), as adopted by CE98. The dotted grid represents loci of constant absorption coefficient (straight lines) and constant spectral slope (curved lines) for the refractive indices of the grains in the particle regolith. For another approach to regolith radiative transfer modeling of spectral data, see Poulet et al. (2002b).

S. Squyres, and M. Showalter. We thank Francois Poulet for helpful comments that improved the manuscript. Difficult-to-find material archived in, and/or easily retrieved from, the Planetary Rings PDS Node, some of it unpublished, was especially useful in preparing this reanalysis. Ironically, some of this was initially provided to the Rings Node by J.N.C., who then retained but has misplaced the original.

References

- Buratti, B.J., 1984. Voyager disk resolved photometry of the saturnian satellites. *Icarus* 59, 392–405.
- Cuzzi, J.N., Estrada, P.R., 1998. Compositional evolution of Saturn's rings due to meteoroid bombardment. *Icarus* 132, 1–35.
- Cuzzi, J.N., French, R.C., Dones, L., Estrada, P.R., Showalter, M.R., 2000. Multicolor photometry of Saturn's main rings from HST and Voyager: color variation with phase and opening angle, location, and optical depth. 32nd DPS Meeting, Pasadena, CA, October 2000. *Bull. Am. Astron. Soc.* 32 (3), 1087.
- Cuzzi, J.N., French, R.C., Dones, L., 2002. HST multicolor (255–1042 nm) photometry of Saturn's main rings. I. Radial profiles, phase and opening angle variations, and regional spectra. *Icarus* 158, 199–223.
- Danielson, G.E., Kupferman, P.N., Johnson, T.V., Soderblom, L.A., 1981. Radiometric performance of the Voyager cameras. *J. Geophys. Res.* 86, 8683–8689.
- Dones, L., Cuzzi, J.N., Showalter, M.R., 1993. Voyager photometry of Saturn's A ring. *Icarus* 105, 184–215.
- Doyle, L., Dones, L., Cuzzi, J.N., 1989. Radiative transfer modeling of Saturn's outer B ring. *Icarus* 80, 104–135.
- Estrada, P., Cuzzi, J.N., 1996. Voyager observations of the color of Saturn's rings. *Icarus* 122, 251–272; Erratum: *Icarus* 125 (1996), 474.
- Karkoschka, E., 1994. Spectrophotometry of the jovian planets and Titan at 300- to 1000-nm wavelength: the methane spectrum. *Icarus* 111, 174–192.
- McFadden, L.A., Bell, J.F., McCord, T.B., 1980. Visible spectral reflectance measurements (0.33–1.0 μ) of the Galilean satellites at many orbital phase angles. *Icarus* 44, 410–430.
- Noll, K.S., Roush, T.L., Cruikshank, D.P., Johnson, R.E., Pendleton, Y.V., 1997. Detection of ozone on Saturn's satellites Rhea and Dione. *Nature* 388, 45–47.
- Poulet, F., Cuzzi, J.N., 2002. The composition of Saturn's rings. *Icarus* 160, 350–358.
- Poulet, F., Karkoschka, E., Sicardy, B., 1999. Spectrophotometry of Saturn's small satellites and rings from Hubble Space Telescope images. *J. Geophys. Res.* 104 (E10), 24095–24110.
- Poulet, F., Cuzzi, J.N., Dones, L., 2000. Modeling the Phase Variation of Saturn's Ring Brightness and Color from HST Observations. DPS, Pasadena.
- Poulet, F., Cuzzi, J.N., French, R.C., Dones, L., 2002a. Modeling the phase variation of Saturn's ring brightness and color from HST observations. *Icarus* 158, 224–248.

- Poulet, F., Cuzzi, J.N., Cruikshank, D., Roush, T., Dalle Ore, C., 2002b. Comparison between the Shkuratov and Hapke scattering theories for solid planetary surfaces: application to the surface composition of two Centaurs. *Icarus* 160, 313–324.
- Showalter, M.R., Bollinger, K.J., Cuzzi, J.N., Nicholson, P.D., 1996. The rings node for the Planetary Data System. *Planet. Space Sci.* 44, 33–45.
- Spencer, J.R., Calvin, W.M., Person, M.J., 1995. CCD spectra of the galilean satellites: molecular oxygen on Ganymede. *J. Geophys. Res.* 100 (E9), 19049–19056.

Statement of ownership, management, and circulation required by the Act of October 23, 1962, Section 4369, Title 39, United States Code: of

ICARUS

Published monthly by Elsevier Inc., 6277 Sea Harbor Drive, Orlando, FL 32887-4900. Number of issues published annually: 12. Editor: P.D. Nicholson, Cornell University, Ithaca, NY 14853-6801, USA.

Owned by Elsevier Inc., 525 B Street, Suite 1900, San Diego, CA 92101-4495. Known bondholders, mortgagees, and other security holders owning or holding 1 percent or more of total amount of bonds, mortgages, and other securities: None.

Paragraphs 2 and 3 include, in cases where the stockholder or security holder appears upon the books of the company as trustee or in any other fiduciary relation, the name of the person or corporation for whom such trustee is acting, also the statements in the two paragraphs show the affiant's full knowledge and belief as to the circumstances and conditions under which stockholders and security holders who do not appear upon the books of the company as trustees, hold stock and securities in a capacity other than that of a bona fide owner. Names and addresses of individuals who are stockholders of a corporation which itself is a stockholder or holder of bonds, mortgages, or other securities of the publishing corporation have been included in paragraphs 2 and 3 when the interests of such individuals are equivalent to 1 percent or more of the total amount of the stock or securities of the publishing corporation.

Total no. copies printed: average no. copies each issue during preceding 12 months: 550; single issue nearest to filing date: 550. Paid circulation (a) to term subscribers by mail, carrier delivery, or by other means: average no. copies each issue during preceding 12 months: 117; single issue nearest to filing date: 120. (b) Sales through agents, news dealers, or otherwise: average no. copies each issue during preceding 12 months: 298; single issue nearest to filing date: 267. Free distribution (a) by mail: average no. copies each issue during preceding 12 months: 74; single issue nearest to filing date: 66. (b) Outside the mail: average no. copies each issue during preceding 12 months: 9; single issue nearest to filing date: 9. Total no. of copies distributed: average no. copies each issue during preceding 12 months: 489; single issue nearest to filing date: 453. Percent paid and/or requested circulation: average percent each issue during preceding 12 months: 84.9%; single issue nearest to filing date: 85.4%.

(Signed) Paul Richmond, Manufacturing and Operations Manager